Received: 31 May 2020 | Revised: 1 September 2020 | Accepted: 2 September 2020

DOI: 10.1002/jrs.5996

SPECIAL ISSUE - RESEARCH ARTICLE

Journal of RAMAN SPECTROSCOPY WILEY

# Helicity-resolved resonant Raman spectroscopy of layered $WS_2$

Yan Zhao[1,2] | Shiyi Han[2] | Jin Zhang[2] | Lianming Tong[2]

[1]Academy for Advanced Interdisciplinary Studies, Peking University, Beijing, China

[2]Center for Nanochemistry, Beijing Science and Engineering Center for Nanocarbons, Beijing National Laboratory for Molecular Sciences, College of Chemistry and Molecular Engineering, Peking University, Beijing, China

**Correspondence**
Jin Zhang and Lianming Tong, Center for Nanochemistry, Beijing Science and Engineering Center for Nanocarbons, Beijing National Laboratory for Molecular Sciences, College of Chemistry and Molecular Engineering, Peking University, Beijing 100871, China.
Email: jinzhang@pku.edu.cn; tonglm@pku.edu.cn

**Funding information**
Beijing National Laboratory for Molecular Sciences, Grant/Award Number: BNLMS-CXTD-202001; National Natural Science Foundation of China, Grant/Award Numbers: 21573004, 21790052, 21974004, 51720105003; Ministry of Science and Technology of the People's Republic of China, Grant/Award Numbers: 2016YFA0200104, 2018YFA0703502

**Abstract**

When excited by circularly polarized light, the Raman scattered light may have the same or opposite helicity as the incident light determined by the helicity selection rule. For two-dimensional (2D) transition metal dichalcogonides (TMDCs), the helicity selection rule can be broken down due to the strong Fröhlich exciton–phonon interaction. However, how the helicity selection rule changes with excitation energy has not been reported yet. Here, we study the helicity-resolved Raman scattering of layered $WS_2$ excited by circularly polarized light for excitations off-excitonic resonance and near resonance to different excitons. We find that for off-resonance excitation, the helicity of $E^1_{2g}$ mode of $WS_2$ obeys the helicity selection rule determined by the symmetry of crystal structure and vibration modes. When excited near resonance to the B exciton, the breakdown of the helicity selection rule is observed, which is attributed to the appearance of nonzero diagonal elements of the Raman tensor resulted from the Fröhlich exciton–phonon interaction. The layer number dependence of the helicity polarization ratio of the $E^1_{2g}$ mode shows that the proportion of helicity-conserved component decreases with the increase of layer number. When the excitation energy is near resonance to the A exciton, the different helicity polarization ratio is found and remains unchanged with increasing layer number, which may be attributed to the different coupling strengths of exciton–phonon interactions.

**KEYWORDS**

excitonic resonance, exciton-phonon coupling, helicity, Raman scattering, $WS_2$

## 1 | INTRODUCTION

Transition metal dichalcogenides (TMDCs) are promising materials for future electronic and photoelectric devices.[1–4] The unique structure and properties of TMDCs have been widely studied by many characterization methods, among which Raman spectroscopy is advantageous for its in-situ, rapid and nondestructive characteristics.[5–7] Polarized Raman spectroscopy (PRS) can reveal the symmetry of crystal lattice. For example, angle-resolved linearly PRS has been widely used to identify the lattice orientation of two-dimensional (2D) crystals.[8–10] Recently, helicity-resolved Raman spectroscopy (HRRS) has been developed to analyze the symmetry of first-order Raman modes in TMDCs.[11] When excited by circularly polarized light, the first-order Raman modes can also be circularly polarized, and the helicity of Raman scattered light can be the same (helicity-conserved) or opposite (helicity-changed) to the incident light.

The helicity of Raman scattered light is determined by the symmetry of crystal and vibration modes, thus the

  

helicity selection rule of first-order Raman modes can be deduced from the Raman tensor. Besides, the conversation law of pseudo-angular momentum (PAM) during the photon–electron and electron–phonon interactions in the Raman scattering process can also be used to analyze the helicity of Raman scattered light.[12] The conversation law of PAM in the Raman scattering process can be expressed by $\sigma_s - \sigma_i = Np_1 - m_v^{ph} + N_V p_2$, where $\sigma_i$ and $\sigma_s$ are the helicities of incident and scattered light, $m_v^{ph}$ is the PAM of phonon, $N$ and $N_V$ are the rotational symmetries of crystal structure and the vibration mode, $p_1$ and $p_2$ are arbitrary integers, respectively. From the equation above, the helicity of Raman scattered light is mainly related to the symmetries of crystal structures and vibration modes, and the PAM of the phonon involved in the Raman scattering. As reported previously, for hexagonal crystals, the degenerate phonons at Γ point are chiral,[13] and the PAM of the phonon is $+\hbar$ or $-\hbar$. Furthermore, the helicity selection rule can also be related to the excitation energy, that is, on- or off-excitonic resonance excitations.[14,15]

$WS_2$ is an important member of TMDCs and has attracted much attention for its distinctive photoemission and excitonic properties.[16] There are two first-order Raman active modes of $WS_2$ for the back-scattering configuration, that is, the $E^1_{2g}$ mode and the $A_{1g}$ mode. The former represents the in-plane vibration of W and S atoms, and the later originates from the out-of-plane vibration of S atoms.[17] There are two main excitons in $WS_2$, namely, A exciton and B exciton, which originate from the splitting of the valence band due to the strong spin-orbit coupling.[18] The energy splitting in $WS_2$ is relatively large as ~0.4 eV,[18–20] so that the A and B exitons do not interfere for all excitation energies, making it an ideal prototype to study the Raman helicity selection rule for different excitation conditions. In this work, we explore the helicity selection rule in $WS_2$ using different excitation energies: 2.54 eV (off-excitonic resonance), 2.41 and 2.33 eV (near resonance to B exciton), and 1.96 eV (near-resonance to A exciton). We find that for off-resonance excitation, the $E^1_{2g}$ mode is helicity-changed and the $A_{1g}$ mode is helicity-conserved, corresponding to the helicity selection rule deduced from the Raman tensor or the conservation law of PAM. However, for near-excitonic resonance excitation, we find that the $E^1_{2g}$ mode is no longer helicity-changed and the helicity-selection rule breaks down, which is consistent with the reported results for $MoS_2$.[14,15,21] This is attributed to the much enhanced Fröhlich interaction for the near-excitonic resonance excitation, leading to the nonzero diagonal Raman tensor elements for the LO phonon.[21–23] Besides, we find that this phenomenon exists not only for monolayer $WS_2$ but also for multilayer $WS_2$. We further measure the helicity-resolved Raman spectra of $WS_2$ with different layer numbers for excitation near-resonance to B exciton and find that the polarization ratio of the $E^1_{2g}$ mode decreases with the increase of layer number, which is due to the increased dielectric screening effect on the exciton. Besides, when changing the excitation energy to be near resonance to A exciton, the polarization ratio of the $E^1_{2g}$ mode is different, and the layer number dependence is not obvious, which may be attributed to the difference in the strength of exciton–phonon coupling.

## 2 | MATERIALS AND METHODS

### 2.1 | Preparation of layered $WS_2$

Layered $WS_2$ is obtained by mechanical exfoliation onto a 300-nm $SiO_2$/Si substrate with the assistance of Scotch tape. Then, the $WS_2$ flakes with different layers are selected using optical microscope (OM, Olympus, BX51). Due to the difference in the reflection contrast, $WS_2$ flakes with different thicknesses exhibit different colors under OM. The thicknesses are characterized by atomic force microscope (AFM, Bruker, Dimension Icon).

### 2.2 | Raman and PL spectroscopy

The photoluminescence (PL) spectroscopy is performed on a confocal Raman microscopy (WITec Alpha300 R) equipped with an Argon ion laser operating at 488 nm. Raman spectra for 488-nm excitation are also measured using the same equipment. Raman scattering measurements using laser energies of 1.96, 2.33, and 2.41 eV are performed using a confocal Raman spectroscope (JY Horiba HR800) in the back-scattering configuration. The incident lasers are focused on the sample by a 100 × objective lens (NA = 0.9), and the laser power is kept below 0.5 mW to avoid damage to materials.

The helicity-resolved Raman spectra are measured by exciting the samples with circularly polarized light and collecting the Raman scattered light of specific helicity. Figure 1 shows the schematic of the optical setup in our experiments. The incident laser is a left- (σ+) or right- (σ−) circularly polarized light that is generated by the linear polarizer I and a quarter-wave plate, and the Raman scattered light passes through the same quarter-wave plate and the linear polarizer II to be detected by the spectrometer. In our experiments, we fix the helicity of incident light (σ+) and select the helicity of Raman scattered light to be the same (σ + σ+) or opposite (σ + σ−) to the incident light. If the Raman intensity for

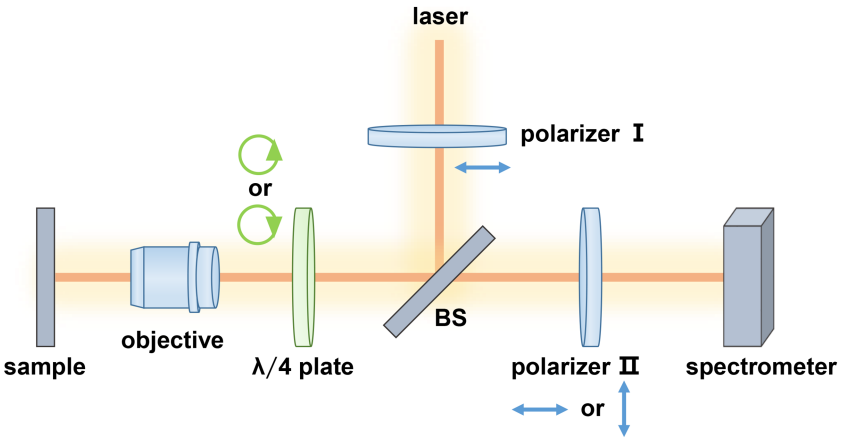


**FIGURE 1** Schematic of the optical setup for helicity-resolved Raman spectroscopy

the σ + σ + configuration is zero and that for the σ + σ− configuration is nonzero, it is called helicity-changed. Conversely, it is called helicity-conserved.

## 3 | RESULTS AND DISCUSSION

### 3.1 | The off-excitonic resonant HRRS of monolayer $WS_2$

Figure 2a shows the optical image of mechanically exfoliated monolayer $WS_2$ on 300-nm $SiO_2$/Si substrate, and the AFM image in Figure 2b shows that the thickness of the $WS_2$ flake is 1.5 nm, a bit larger than the thickness of monolayer $WS_2$ reported previously,[24] which may be attributed to the larger space between the flake and the substrate. The measurement of PL spectrum further confirms the monolayer $WS_2$ because there is a strong emission peak corresponding to the direct bandgap transition, and there is no peak from indirect bandgap transition, which is a typical feature for bilayer or multilayer $WS_2$.[19] As shown in Figure 2c, there are two emission peaks in the spectral range from 488 to 750 nm, which correspond to the A exciton (∼635 nm, 1.95 eV) and the B exciton (∼527 nm, 2.35 eV), respectively.

We then measured the off-excitonic resonant HRRS of monolayer $WS_2$ by the excitation energy $E_L = 2.54$ eV (wavelength of 488 nm). As shown in Figure 2d, the $E^1_{2g}$ mode is helicity-changed, and the $A_{1g}$ mode is helicity-conserved. This result is consistent with the helicity selection rule deduced by the Raman tensor calculation. The Raman intensity can be calculated by $I \propto \left|\sigma_s^{\dagger} \cdot R \cdot \sigma_i\right|^2$, where $R$ is the Raman tensor and $\sigma_i$ and $\sigma_s$ are the helicities of the incident and the Raman scattered light, respectively. The $E^1_{2g}$ mode is a doubly degenerate mode of iLO and iTO phonons, and the $A_{1g}$ mode is from the ZO phonon at Γ point.[11] The Raman tensors for $E^1_{2g}$ and $A_{1g}$ modes are[6]

$$E^1_{2g}: \begin{pmatrix} d & 0 & 0 \\ 0 & -d & 0 \\ 0 & 0 & 0 \end{pmatrix}, \begin{pmatrix} 0 & d & 0 \\ d & 0 & 0 \\ 0 & 0 & 0 \end{pmatrix}; A1g: \begin{pmatrix} a & 0 & 0 \\ 0 & a & 0 \\ 0 & 0 & b. \end{pmatrix}.$$

The left- and right-circularly polarized light can be represented by Jones vectors. For left-circularly polarized light, $\sigma+ = \frac{1}{\sqrt{2}} \begin{pmatrix} 1 \\ i \\ 0 \end{pmatrix}$. For right-circularly polarized light, $\sigma- = \frac{1}{\sqrt{2}} \begin{pmatrix} 1 \\ -i \\ 0 \end{pmatrix}$. The calculation results for monolayer and bilayer $WS_2$ are listed in Table S1.

### 3.2 | The near-excitonic resonant HRRS of monolayer $WS_2$

In the resonant Raman spectrum of $WS_2$ excited by 2.41 eV laser, there are several second-order Raman peaks, as shown in Figure 3a. In order to extract the intensities of the $E^1_{2g}$ and $A_{1g}$ modes, these peaks are fitted by Lorentz line shapes, and the peak positions and the assignments are listed in Table S2. The HRRS of monolayer $WS_2$ is measured using the excitation energy $E_L = 2.41$ eV and 2.33 eV, which are both near-resonant to B exciton. As shown in Figure 3b,c, the $A_{1g}$ mode is helicity-conserved, which is consistent with the result for off-resonance excitation. However, for the $E^1_{2g}$ mode, the intensities for the σ + σ + and σ + σ− configurations are both nonzero. Thus, the helicity selection rule for $E^1_{2g}$ mode under near-excitonic resonance excitation is different from the off-resonance condition. The breakdown of helicity selection rule for resonant Raman scattering has been reported in $MoS_2$,[14,15] which originates from the Fröhlich electron–phonon coupling.[21] The Fröhlich interaction is generated by the LO phonon in polar or

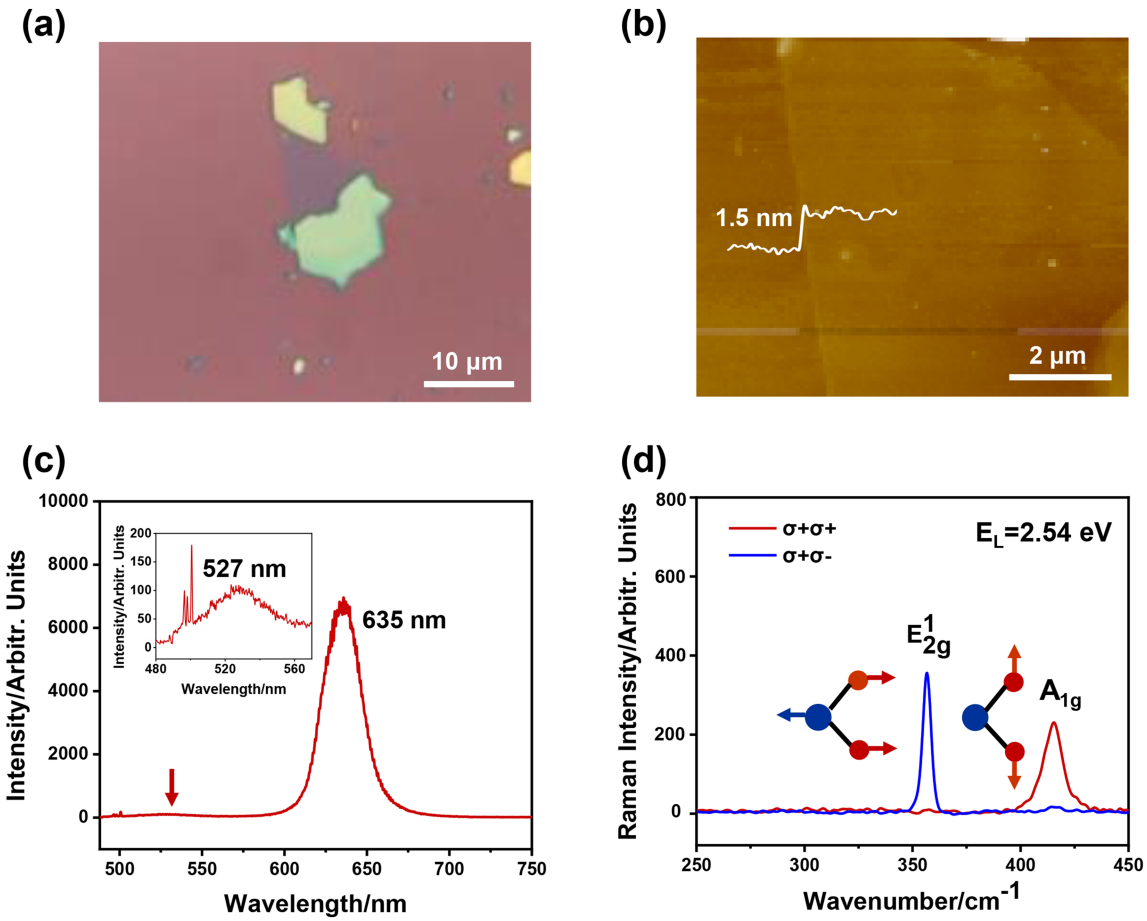


**FIGURE 2** (a) The optical image of mechanically exfoliated monolayer $WS_2$. (b) The thickness of monolayer $WS_2$ (~1.5 nm) measured by atomic force microscope (AFM). (c) Photoluminescence (PL) spectrum of monolayer $WS_2$, excited by $E_L = 2.54$ eV (488 nm) laser. The peak at 635 nm (1.95 eV) corresponds to the A exciton. Inset is an enlarged view of the B exciton at 527 nm (2.35 eV), corresponding to the peak position indicated by the red arrow. (d) Helicity-resolved Raman spectra of monolayer $WS_2$ excited by $E_L = 2.54$ eV laser, which show that the $E^1_{2g}$ mode is helicity-changed and the $A_{1g}$ mode is helicity-conserved. Inset shows the atomic vibrations of the two first-order Raman modes

ionic crystals.[25] The strength of Fröhlich interaction is much enhanced on resonance to the excitonic energy level and induces the nonzero diagonal Raman tensor elements for $E^1_{2g}$ mode,[22,26] thus results in the nonzero intensity for σ + σ + configuration. The form of Raman tensor for $E^1_{2g}$ mode changed by the Fröhlich interaction and the derivation process of the helicity selection rule are shown in Note S1. The similar phenomena for $WS_2$ in this work reflect that the Fröhlich exciton–phonon interaction can also be prominent in $WS_2$. In order to compare the relative proportion of the Raman intensities for σ + σ + and σ + σ− configurations, we define the polarization ratio as

$$\rho = \frac{I_{\sigma+\sigma+} - I_{\sigma+\sigma-}}{I_{\sigma+\sigma+} + I_{\sigma+\sigma-}},$$

which is related to the strength of Fröhlich interaction. The polarization ratio for $E_L = 2.41$ and 2.33 eV is calculated to be 0.51 and 0.17, respectively.

In order to confirm the influence of exciton-LO phonon coupling on the polarization selection rule, we further measured the linearly polarized Raman spectra of $WS_2$ for near-excitonic resonance excitation by $E_L = 2.33$ eV, and the optical setup is shown in Figure S1 and the experimental results are shown in Figure S3. The intensities of $E^1_{2g}$ mode in XX and XY configurations are equal for off-resonant excitation, whereas they are different for resonant excitation. The linear polarization selection rules of $E^1_{2g}$ mode for off-resonant and resonant excitations are shown in Note S2. The results above indicate that when considering the Raman polarization selection rule in polar or ionic 2D crystals such as TMDCs, the Fröhlich interaction should not be neglected.

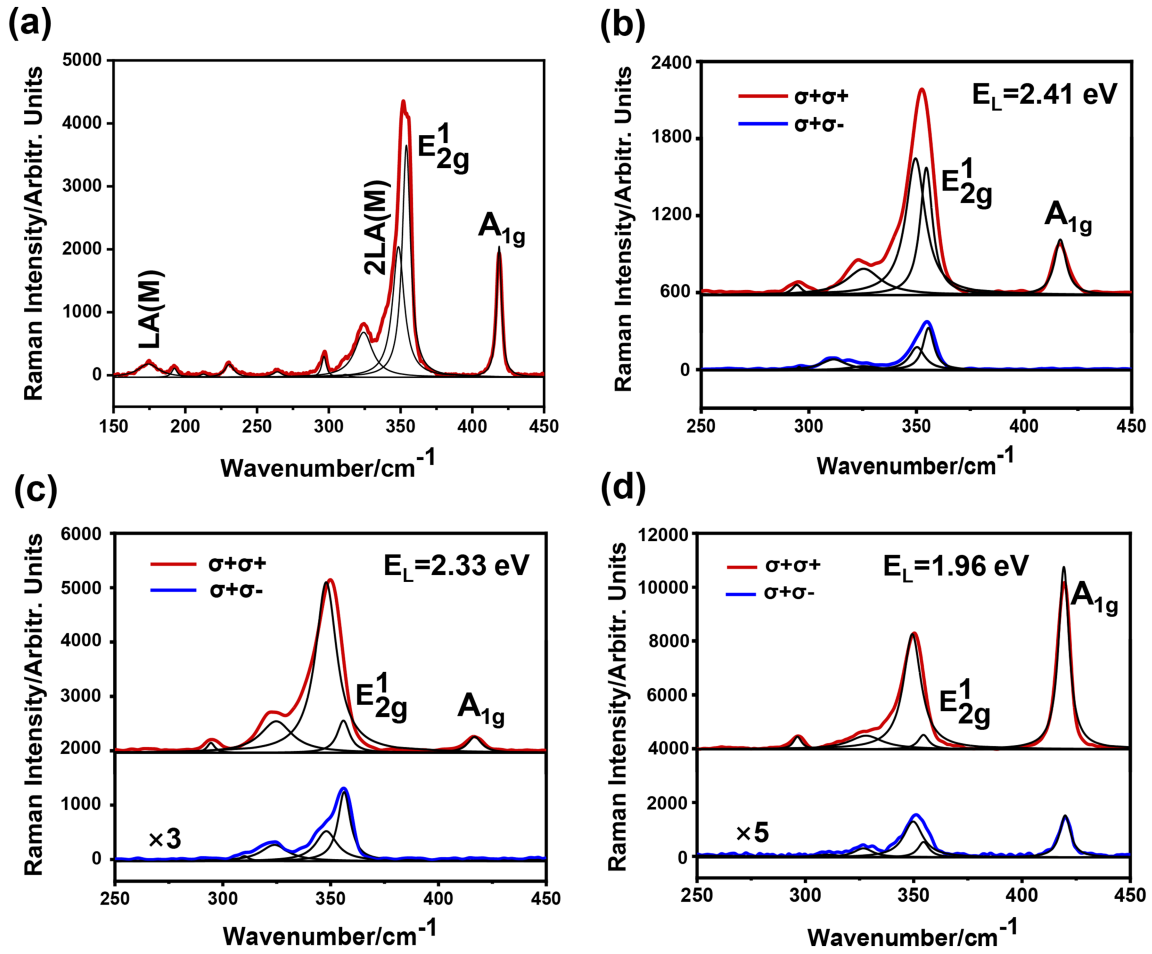


**FIGURE 3** (a) The resonant Raman spectrum of monolayer $WS_2$, excited by $E_L$ = 2.41 eV laser. All the peaks are fitted by Lorentz line shapes. (b and c) The helicity-resolved Raman spectra (HRRS) of monolayer $WS_2$, the excitation energy is (b) 2.41 and (c) 2.33 eV. (d) The HRRS of bilayer $WS_2$, excited by $E_L$ = 1.96 eV. All the peaks are fitted by Lorentz line shapes

We also measured the HRRS near resonance to the A exciton by $E_L$ = 1.96 eV. Because of the strong PL background in the Raman spectra for monolayer $WS_2$, we select the bilayer $WS_2$ flake for the HRRS, and the optical and AFM images are shown in Figure S2. As shown in Figure 3d, the $E^1_{2g}$ mode also appears for the σ + σ + configuration, and the intensity of helicity-changed component is rather weak compared with the helicity-conserved component. The polarization ratio is calculated to be 0.8, which indicates that the strength of Fröhlich interaction is large.

## 3.3 | The layer number dependence of HRRS for $WS_2$

The helicity selection rule of $E^1_{2g}$ mode in resonant HRRS is also valid for multilayer $WS_2$. We measure the HRRS of $WS_2$ with different layers with the excitation energy $E_L$ = 2.41 and 1.96 eV that are near resonance to B and A excitons, as shown in Figure 4a,b, respectively. The $WS_2$ flakes used in the experiments are shown in Figure S2. For $WS_2$ with different layers, the variation of the peak positions of A and B excitons is slight,[20] thus the excitation laser energies $E_L$ = 2.41 and 1.96 eV are still near resonance to the excitons.

As shown in Figure 4c, for $E_L$ = 2.41 eV, with the increase of layer number, the polarization ratio of $A_{1g}$ mode remains at ∼1, which means that the $A_{1g}$ mode remains helicity-conserved. Whereas the $E^1_{2g}$ mode exists for both σ + σ + and σ + σ− configurations for $WS_2$ with different layer numbers, which reflects that the Fröhlich exciton–phonon interaction is also prominent in multilayer $WS_2$. It is worth noting that the polarization ratio of $E^1_{2g}$ mode decreases with the increase of layer number. This can be explained by the increase of dielectric screening effect on the excitons with the increase of layer number.[27–29] Besides, we also measured the dependence of linearly polarized Raman spectra of $WS_2$ on the layer number for the resonant excitation ($E_L$ = 2.33 eV), as shown in Figure S3. The polarization ratio of $E^1_{2g}$ mode decreases with the increase of layer number, as shown in

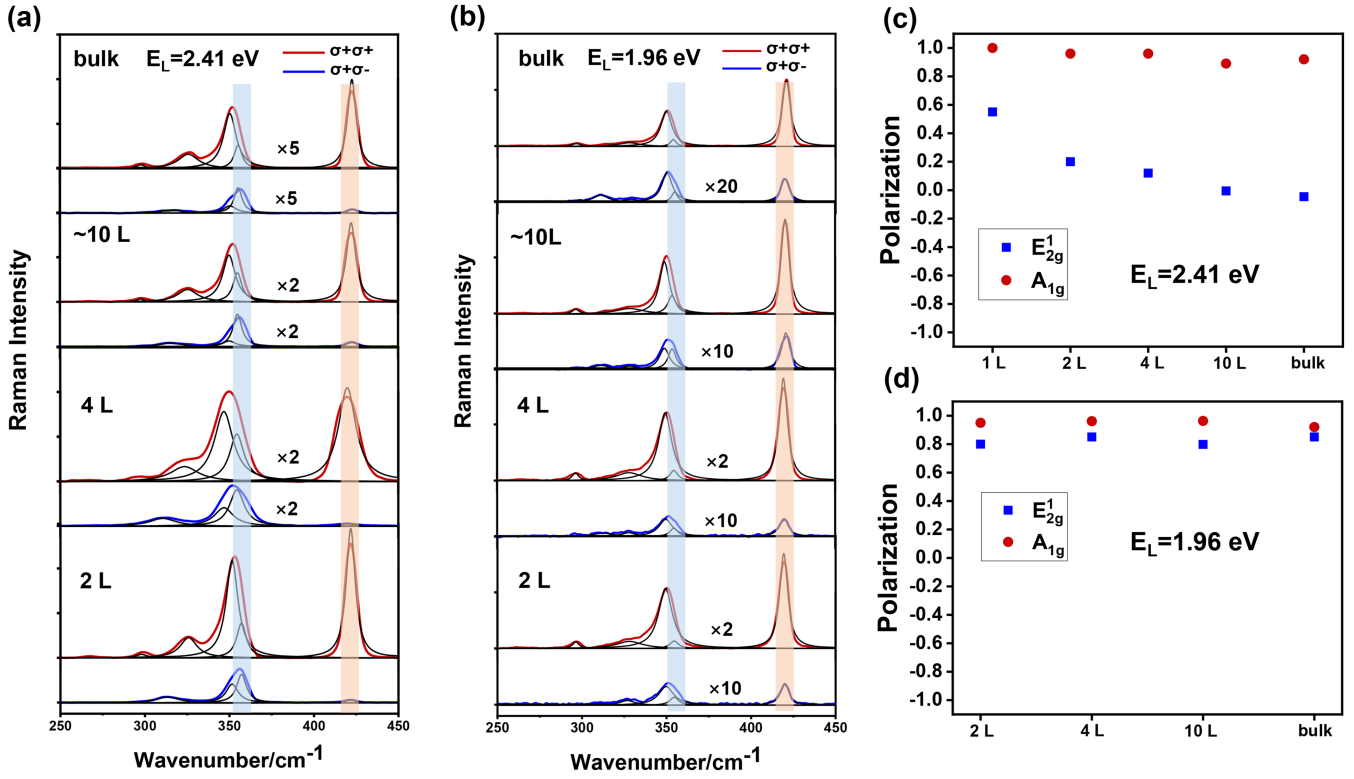


**FIGURE 4** (a and b) The helicity-resolved Raman spectra for $WS_2$ with different layer numbers, excited by (a) $E_L = 2.41$ eV and (b) $E_L = 1.96$ eV laser. (c and d) The polarization ratios for $E^1_{2g}$ mode and $A_{1g}$ mode, corresponding to (c) $E_L = 2.41$ eV and (d) $E_L = 1.96$ eV excitation

Figure S4, which is consistent with the evolution of the helicity polarization ratio.

For $E_L = 1.96$ eV, the polarization ratio of $E^1_{2g}$ mode for multilayer $WS_2$ is higher than that for $E_L = 2.41$ eV, and the layer number dependence is not obvious. This may originate from the different strengths of Fröhlich exciton–phonon interaction when the excitation energy is near resonance to different exciton energy levels.[26,30] The transition matrix elements can be different for different exciton states, leading to various exciton–phonon interactions. Besides, it has been reported that the change of layer number of $WS_2$ has an obvious influence on the energy of 2s exciton whereas the 1s exciton remains relatively unchanged.[31] Thus for different excitonic states, the dielectric screening effect on the exciton transition energy can be different, which may lead to the weaker dependence of polarization ratio on the layer number for 1.96-eV excitation.

## 4 | CONCLUSIONS

The HRRS can be used to identify the symmetry of crystal structure and vibration modes. However, the helicity selection rule can be affected by the exciton–phonon interaction and can be broken down for on-excitonic resonance excitations. In the present work, we measured the HRRS of layered $WS_2$ with the excitation energy off- and near-resonance to the excitonic energy levels. We find that the $E^1_{2g}$ mode disobeys the helicity selection rule determined by the classic symmetry analysis for the resonant excitation and should consider the diagonal Raman tensor elements of the LO phonon induced by the Fröhlich exciton–phonon interaction. These results indicate that the exciton plays an important role in the resonance Raman spectroscopy, which not only affects the intensity of Raman peaks but also may change the Raman selection rule. We further measure the HRRS of $WS_2$ flakes with different layer numbers and find that the polarization ratio of $E^1_{2g}$ mode decreases with the increase of layer number because the dielectric screening effect on the excitons becomes stronger for multilayer $WS_2$. Besides, the polarization ratio of $E^1_{2g}$ mode shows difference when the excitation energy is near resonance to A exciton, which reflects that the strength of exciton–phonon coupling varies for different excitons, and the exciton type would also affect the helicity of Raman scattered light. This work could give a better understanding on the role of different electron–phonon and exciton–phonon couplings in Raman spectroscopy and indicate that HRRS could be used to study the excitonic effects in Raman scattering.

## ACKNOWLEDGEMENTS

This work was financially supported by Beijing National Laboratory for Molecular Sciences (BNLMS-CXTD-202001), the Ministry of Science and Technology of the People's Republic of China (2016YFA0200104 and 2018YFA0703502) and the National Natural Science Foundation of China (Grant 51720105003, 21790052, 21573004, and 21974004).

## ORCID

*Jin Zhang* https://orcid.org/0000-0003-3731-8859
*Lianming Tong* https://orcid.org/0000-0001-7771-4077

## REFERENCES

[1] B. Radisavljevic, A. Radenovic, J. Brivio, V. Giacometti, A. Kis, *Nat. Nanotechnol.* **2011**, *6*, 147.
[2] Q. H. Wang, K. Kalantar-Zadeh, A. Kis, J. N. Coleman, M. S. Strano, *Nat. Nanotechnol.* **2012**, *7*, 699.
[3] K. F. Mak, J. Shan, *Nat. Photonics* **2016**, *10*, 216.
[4] N. Perea-Lopez, A. L. Elias, A. Berkdemir, A. Castro-Beltran, H. R. Gutierrez, S. Feng, R. Lv, T. Hayashi, F. Lopez-Urias, S. Ghosh, B. Muchharla, S. Talapatra, H. Terrones, M. Terrones, *Adv. Funct. Mater.* **2013**, *23*, 5511.
[5] X. Zhang, X.-F. Qiao, W. Shi, J.-B. Wu, D.-S. Jiang, P.-H. Tan, *Chem. Soc. Rev.* **2015**, *44*, 2757.
[6] R. Loudon, *Adv. Phys.* **2001**, *50*, 813.
[7] S. Zhang, N. Zhang, Y. Zhao, T. Cheng, X. Li, R. Feng, H. Xu, Z. Liu, J. Zhang, L. Tong, *Chem. Soc. Rev.* **2018**, *47*, 3217.
[8] J. Wu, N. Mao, L. Xie, H. Xu, J. Zhang, *Angew. Chem., Int. Ed.* **2015**, *54*, 2366.
[9] M. Zhu, Y. Zhao, Q. Feng, H. Lu, S. Zhang, N. Zhang, C. Ma, J. Li, J. Zheng, J. Zhang, H. Xu, T. Zhai, J. Zhao, *Small* **2019**, *15*, 1903159.
[10] S. Cao, W. Ma, G. Zhai, Z. Xie, X. Gao, Y. Zhao, X. Ma, L. Tong, S. Jia, J.-H. Chen, *J. Phys.: Condens. Matter* **2020**, *32*, 12LT01.
[11] S.-Y. Chen, C. Zheng, M. S. Fuhrer, J. Yan, *Nano Lett.* **2015**, *15*, 2526.
[12] Y. Tatsumi, T. Kaneko, R. Saito, *Phys. Rev. B* **2018**, *97*, 195444.
[13] L. Zhang, Q. Niu, *Phys. Rev. Lett.* **2015**, *115*, 115502.
[14] S. G. Drapcho, J. Kim, X. Hong, C. Jin, S. Shi, S. Tongay, J. Wu, F. Wang, *Phys. Rev. B* **2017**, *95*, 165417.
[15] N. Yoshikawa, S. Tani, K. Tanaka, *Phys. Rev. B* **2017**, *95*, 115419.
[16] C. Cong, J. Shang, Y. Wang, T. Yu, *Adv. Opt. Mater.* **2018**, *6*, 1700767.
[17] A. Berkdemir, H. R. Gutierrez, A. R. Botello-Mendez, N. Perea-Lopez, A. L. Elias, C.-I. Chia, B. Wang, V. H. Crespi, F. Lopez-Urias, J.-C. Charlier, H. Terrones, M. Terrones, *Sci. Rep.* **2013**, *3*, 1755.
[18] A. Ramasubramaniam, *Phys. Rev. B* **2012**, *86*, 115409.
[19] W. Zhao, Z. Ghorannevis, L. Chu, M. Toh, C. Kloc, P.-H. Tan, G. Eda, *ACS Nano* **2013**, *7*, 791.
[20] H. Zeng, G.-B. Liu, J. Dai, Y. Yan, B. Zhu, R. He, L. Xie, S. Xu, X. Chen, W. Yao, X. Cui, *Sci. Rep.* **2013**, *3*, 1608.
[21] B. Miller, J. Lindlau, M. Bommert, A. Neumann, H. Yamaguchi, A. Holleitner, A. Hoegele, U. Wurstbauer, *Nat. Commun.* **2019**, *10*, 807.
[22] R. M. Martin, T. C. Damen, *Phys. Rev. Lett.* **1971**, *26*, 86.
[23] C. Trallero-Giner, A. Cantarero, M. Cardona, *Phys. Rev. B* **1989**, *40*, 4030.
[24] H. R. Gutierrez, N. Perea-Lopez, A. L. Elias, A. Berkdemir, B. Wang, R. Lv, F. Lopez-Urias, V. H. Crespi, H. Terrones, M. Terrones, *Nano Lett.* **2013**, *13*, 3447.
[25] H. Fröhlich, *Proc. R. Soc. Lond. A.* **1952**, *215*, 291.
[26] R. M. Martin, *Phys. Rev. B* **1971**, *4*, 3676.
[27] H.-P. Komsa, A. V. Krasheninnikov, *Phys. Rev. B* **2012**, *86*, 241201.
[28] E. J. G. Santos, E. Kaxiras, *ACS Nano* **2013**, *7*, 10741.
[29] T. Cheiwchanchamnangij, W. R. L. Lambrecht, *Phys. Rev. B* **2012**, *85*, 205302.
[30] N. F. Hinsche, A. S. Ngankeu, K. Guilloy, S. K. Mahatha, A. G. Cabo, M. Bianchi, M. Dendzik, C. E. Sanders, J. A. Miwa, H. Bana, E. Travaglia, P. Lacovig, L. Bignardi, R. Larciprete, A. Baraldi, S. Lizzit, K. S. Thygesen, P. Hofmann, *Phys. Rev. B* **2017**, *96*, 121402.
[31] A. Chernikov, T. C. Berkelbach, H. M. Hill, A. Rigosi, Y. Li, O. B. Aslan, D. R. Reichman, M. S. Hybertsen, T. F. Heinz, *Phys. Rev. Lett.* **2014**, *113*, 076802.

## SUPPORTING INFORMATION

Additional supporting information may be found online in the Supporting Information section at the end of this article.

**How to cite this article:** Zhao Y, Han S, Zhang J, Tong L. Helicity-resolved resonant Raman spectroscopy of layered $WS_2$. *J Raman Spectrosc*. 2020;1–7. https://doi.org/10.1002/jrs.5996